Design and performance analysis of the low-frequency and broadband piezoelectric energy harvester

Laizhao J[1,2], Rui H[1,2] and Weike W[1,2]

[1] School of Mechanical Engineering, Shandong University, Ji'nan 250061, China;
[2] Key Lab. of High Efficiency and Clean Mechanical Manufacture (Shandong University) Ministry of Education, Ji'nan 250061, China

jinglaizhao@126.com

Abstract. A novel type energy harvester composed with n masses and n beams was proposed to solve the problems of high-frequency and narrow band of cantilever energy harvester to improve its energy conversion efficiency, and broaden its application. Firstly, We taken micro beam as the research object, improved its dynamic model with size effect, then verified it by experiments. Secondly, the dynamic model was established based on the improved one, and its response and the output voltage of the external excitation was deduced formula. Finally, the performance was studied when n=2. The results show that resonance frequency was obvious reduced, and there are two frequency points less than 50Hz, 15.25 Hz and 23.08 Hz. Moreover, when the effective output voltage reached 80 mv, the effective frequency band was 20.32 Hz, which can make up for the energy conversion efficiency of single resonant frequency harvester.

1. Introduction

Since the P Curie and J Curie brothers discovered the positive / inverse piezoelectric effect of crystal by experiment, many scholars and research institutes have begun to try to apply it to real life, as a result, the piezoelectric energy conversion technology has been rapidly developed and cantilever energy harvester thereof emerges[1-3]. In 2005, Jeon[4]designed a PZT film-based collector, whose resonant frequency was tested to be 13.9KHz. Wu Xiaoming et al[5] took monocrystalline silicon as the material of cantilever beam and pasted thin piezoelectric material on its surface. At the end of the cantilever beam, they pasted mass blocks prepared by wet etching to form a silicon-based piezoelectric cantilever energy harvester, for which the resonant frequency was 1673Hz. Renaud[6] used AIN-based cantilever got the resonant frequency was 1.8KHz. And its output power was 40μW with an external excitation of 180nm. Gafforelli[7] established a three-layer structured mathematical model for cantilever beam vibration energy harvester. Combined the analytical method and finite element analysis method, he analyzed the mechanical property of harvester, and the results of two different methods were similar, namely the resonant frequency were 1kHz. Fang[8] pasted nickel masses at the end of the cantilever beam to reduce its resonant frequency, and the final value was 608Hz.

It's found by statistics that frequency of ambient vibration energy mainly distributes within a range of 300Hz, however, the resonant frequencies of harvesters in literature [4-8] are higher than 300Hz[9,10], as a result, the harvesters can't be effectively stimulated, nor can they convert mechanical vibration energy into electric energy, thus the propose of power supply fails. At the same time, these harvesters can only convert energy effectively at the resonant frequency, the working band is quite narrow. Therefore, this paper designed a new energy harvester while considering the demands of low resonant

frequency and wide working band. The dynamic performance of the equipment under the influence of scale effect has been studied.

2. Dynamic Performance Analysis of New Energy Harvester

New energy harvester is a new structure consist of n beams and n lumped mass block, as shown in figure.1. With m_i(i=1,2,…,n) referring the quality, m_n locates to the end of the cantilever beam. The whole cantilever beam is divided into n sections by the location of each additional mass, the length and stiffness of each beam is marked as l_i and E_iI_i(i=1,2,…,n). Each straight beam is a composite beam, that is to say PZT piezoelectric coating and Cu electrode are attached on the upper and lower surfaces of Si base beam.

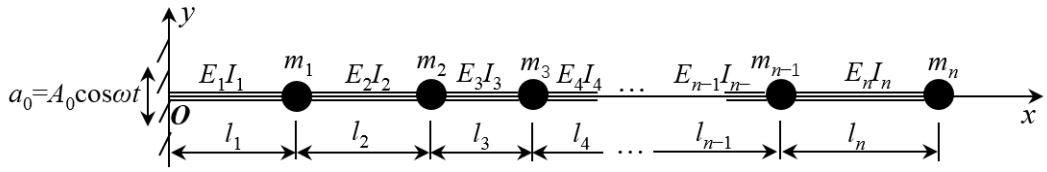

Figure 1. Schematic Diagram of Cantilever Beam With Additional Lumped Mass

It's known that the fixed end O of cantilever beam is given a ground vibration excitation, whose acceleration is $a_0=A_0\cos\omega t$. $w_i\ (x,t)$ (i=1,2,…,n) is taken to describe the transverse vibration displacement of each beam under the excitation of acceleration. According to [11], $w_i\ (x,t)$meets the following differential equation:

$$\rho_i A_i w_{i,tt} + \left(E_i I_i + \mu A_i l^2\right) w_{i,xxxx} = 0 \quad (i = 1,2,...,n) \tag{1}$$

$$w_1(x_0,t) = -A_0 e^{j\omega t}/\omega^2 \qquad w_{1,x}(x_0,t) = 0 \tag{2}$$

At $x_i = \sum_{k=1}^{i} l_k$ (i<n)

$$w_i(x_i,t) = w_{i+1}(x_i,t) \quad w_{i,x}(x_i,t) = w_{i+1,x}(x_i,t) \tag{3}$$

$$\left(E_i I_i + \mu A_i l^2\right) w_{i,xx}(x_i,t) = \left(E_{i+1} I_{i+1} + \mu A_{i+1} l^2\right) w_{i+1,xx}(x_i,t) \tag{4}$$

$$\left(E_i I_i + \mu A_i l^2\right) w_{i,xxx}(x_i,t) = \left(E_{i+1} I_{i+1} + \mu A_{i+1} l^2\right) w_{i+1,xxx}(x_i,t) + m_i w_{i,tt}(x_i,t) \tag{5}$$

At $x_n = \sum_{k=1}^{n} l_k$ (i<n)

$$\begin{aligned} \left(E_n I_n + \mu A_n l^2\right) w_{n,xx}(x_n,t) &= 0 \\ \left(E_n I_n + \mu A_n l^2\right) w_{n,xxx}(x_n,t) &= m_n w_{n,tt}(x_n,t) \end{aligned} \tag{6}$$

Taking a Fourier transformation on formula (1):

$$W_{i,xxxx}(x,\omega) - \lambda_i^4 W_i(x,\omega) = 0 \quad (i = 1,2,...,n) \tag{7}$$

The $\lambda_i^4 = \rho_i A_i \omega^2 (E_i I_i + \mu A_i l^2)^{-1}$ in formula (7) has a general solution $W_i(x,\omega)$ as the following form:

$$W_i(x,\omega) = C_{i1} e^{-j\lambda_i x} + C_{i2} e^{-\lambda_i x} + C_{i3} e^{j\lambda_i x} + C_{i4} e^{\lambda_i x} \tag{8}$$

Under the harmonic excitation, the vibration displacement $w_i\ (x,t)$ of beam i can be marked as:

$$w_i(x,t) = W_i(x,\omega) e^{j\omega t} = \begin{bmatrix} e^{j(\omega t - \lambda_i x)} & e^{-\lambda_i x + j\omega t} \end{bmatrix} \begin{bmatrix} C_{i1} \\ C_{i2} \end{bmatrix} + \begin{bmatrix} e^{j(\omega t + \lambda_i x)} & e^{\lambda_i x + j\omega t} \end{bmatrix} \begin{bmatrix} C_{i3} \\ C_{i4} \end{bmatrix} \tag{9}$$

Front half part of right equation in formula (9) refers to the flexural wave of composite beam along the positive x axis, the latter part refers to the negative flexural wave.

As for each beam, the section corner $w_{i,x}$ is referred to as:

$$w_{i,x}(x,t) = \begin{bmatrix} -j\lambda_i e^{j(\omega t - \lambda_i x)} & -\lambda_i e^{-\lambda_i x + j\omega t} \end{bmatrix} \begin{bmatrix} C_{i1} \\ C_{i2} \end{bmatrix} + \begin{bmatrix} j\lambda_i e^{j(\omega t + \lambda_i x)} & \lambda_i e^{\lambda_i x + j\omega t} \end{bmatrix} \begin{bmatrix} C_{i3} \\ C_{i4} \end{bmatrix} \tag{10}$$

Bending moment of section $M_{i,x}(x,t)$is:

$$M_i(x,t)=\left(E_iI_i+\mu A_il^2\right)W_{i,xx}(x,\omega)e^{j\omega t}=\left(E_iI_i+\mu A_il^2\right)\left(\begin{bmatrix}-\lambda_i^2e^{j(\omega t-\lambda_ix)} & \lambda_i^2e^{-\lambda_ix+j\omega t}\\ -\lambda_i^2e^{j(\omega t+\lambda_ix)} & \lambda_i^2e^{\lambda_ix+j\omega t}\end{bmatrix}\begin{bmatrix}C_{i1}\\C_{i2}\end{bmatrix}+\begin{bmatrix}C_{i3}\\C_{i4}\end{bmatrix}\right) \tag{11}$$

Section shear $Q_{i,x}(x,t)$is:

$$Q_i(x,t)=\left(E_iI_i+\mu A_il^2\right)W_{i,xxx}(x,\omega)e^{j\omega t}=\left(E_iI_i+\mu A_il^2\right)\left(\begin{bmatrix}j\lambda_i^3e^{j(\omega t-\lambda_ix)} & -\lambda_i^3e^{-\lambda_ix+j\omega t}\\ -j\lambda_i^3e^{j(\omega t+\lambda_ix)} & \lambda_i^3e^{\lambda_ix+j\omega t}\end{bmatrix}\begin{bmatrix}C_{i1}\\C_{i2}\end{bmatrix}+\begin{bmatrix}C_{i3}\\C_{i4}\end{bmatrix}\right) \tag{12}$$

Defining:

$$\boldsymbol{C}_i^+=\begin{bmatrix}C_{i1}\\C_{i2}\end{bmatrix},\quad \boldsymbol{C}_i^-=\begin{bmatrix}C_{i3}\\C_{i4}\end{bmatrix},\quad \boldsymbol{e}_i^+=\begin{bmatrix}e^{-j\lambda_ix} & 0\\ 0 & e^{-\lambda_ix}\end{bmatrix},\quad \boldsymbol{e}_i^-=\begin{bmatrix}e^{j\lambda_ix} & 0\\ 0 & e^{\lambda_ix}\end{bmatrix},\quad \boldsymbol{\lambda}_{Wi}^+=\begin{bmatrix}1 & 1\\ -j\lambda_i & -\lambda_i\end{bmatrix},\quad \boldsymbol{\lambda}_{Wi}^-=\begin{bmatrix}1 & 1\\ j\lambda_i & \lambda_i\end{bmatrix}$$

$$\boldsymbol{\lambda}_{Fi}^+=\left(E_iI_i+\mu A_il^2\right)\lambda_i^2\begin{bmatrix}-1 & 1\\ j\lambda_i & -\lambda_i\end{bmatrix},\quad \boldsymbol{\lambda}_{Fi}^-=\left(E_iI_i+\mu A_il^2\right)\lambda_i^2\begin{bmatrix}-1 & 1\\ -j\lambda_i & \lambda_i\end{bmatrix}$$

Taking formula (9) and (10) into formula (2), we can get:

$$\boldsymbol{\lambda}_{W1}^+\boldsymbol{C}_i^++\boldsymbol{\lambda}_{W1}^-\boldsymbol{C}_i^-=\begin{bmatrix}-A_0/\omega^2\\0\end{bmatrix} \tag{13}$$

Taking formula (11) and (12) into formula (4) and (5), we can get:

$$\boldsymbol{\lambda}_{Fi}^+\boldsymbol{e}_i^+(x_i)\boldsymbol{C}_i^++\boldsymbol{\lambda}_{Fi}^-\boldsymbol{e}_i^-(x_i)\boldsymbol{C}_i^--\boldsymbol{\lambda}_{Fi+1}^+\boldsymbol{e}_{i+1}^+(x_i)\boldsymbol{C}_{i+1}^+-\boldsymbol{\lambda}_{Fi+1}^-\boldsymbol{e}_{i+1}^-(x_i)\boldsymbol{C}_{i+1}^-=\begin{bmatrix}0\\-\omega^2m_iW_i(x_i,\omega)\end{bmatrix} \tag{14}$$

In the derivation of formula (14), the relationship between formula (1) and (7) has been cited for the following transformation:

$$\begin{aligned}w_{i,tt}(x,t)&=-\left(E_iI_i+\mu A_il^2\right)w_{i,xxxx}(\rho_iA_i)^{-1}=-\left(E_iI_i+\mu A_il^2\right)W_{i,xxxx}(x,\omega)e^{j\omega t}(\rho_iA_i)^{-1}\\&=-\left(E_iI_i+\mu A_il^2\right)\lambda_i^4W_i(x,\omega)e^{j\omega t}(\rho_iA_i)^{-1}=-\omega^2W_i(x,\omega)e^{j\omega t}\end{aligned}$$

Taking it into formula (9) and we can get:

$$\left(\boldsymbol{\lambda}_{Fi}^+-\boldsymbol{\lambda}_{Fi}\right)\boldsymbol{e}_i^+(x_i)\boldsymbol{C}_i^++\left(\boldsymbol{\lambda}_{Fi}^--\boldsymbol{\lambda}_{Fi}\right)\boldsymbol{e}_i^-(x_i)\boldsymbol{C}_i^--\boldsymbol{\lambda}_{Fi+1}^+\boldsymbol{e}_{i+1}^+(x_i)\boldsymbol{C}_{i+1}^+-\boldsymbol{\lambda}_{Fi+1}^-\boldsymbol{e}_{i+1}^-(x_i)\boldsymbol{C}_{i+1}^-=\begin{bmatrix}0\\0\end{bmatrix} \tag{15}$$

Combined the formula (13), (14) and (15):

$$\begin{bmatrix}A_{11} & A_{12} & 0 & 0 & 0 & 0 & \cdots & 0 & 0 & 0 & 0\\ A_{21} & A_{22} & A_{23} & A_{24} & 0 & 0 & \cdots & 0 & 0 & 0 & 0\\ A_{31} & A_{32} & A_{33} & A_{34} & 0 & 0 & \cdots & 0 & 0 & 0 & 0\\ 0 & 0 & A_{43} & A_{44} & A_{45} & A_{46} & \cdots & 0 & 0 & 0 & 0\\ 0 & 0 & A_{53} & A_{54} & A_{55} & A_{56} & \cdots & 0 & 0 & 0 & 0\\ \vdots & \vdots & \vdots & \vdots & \vdots & \vdots & \ddots & \vdots & \vdots & \vdots & \vdots\\ 0 & 0 & 0 & 0 & 0 & 0 & \cdots & A_{2n-2,2n-3} & A_{2n-2,2n-2} & A_{2n-2,2n-1} & A_{2n-2,2n}\\ 0 & 0 & 0 & 0 & 0 & 0 & \cdots & A_{2n-1,2n-3} & A_{2n-1,2n-2} & A_{2n-1,2n-1} & A_{2n-1,2n}\\ 0 & 0 & 0 & 0 & 0 & 0 & \cdots & 0 & 0 & A_{2n,2n-1} & A_{2n,2n}\end{bmatrix}\begin{bmatrix}C_1^+\\C_1^-\\C_2^+\\C_2^-\\\vdots\\C_{n-1}^+\\C_{n-1}^-\\C_n^+\\C_n^-\end{bmatrix}=\begin{bmatrix}\boldsymbol{g}\\0\\0\\0\\0\\\vdots\\0\\0\\0\end{bmatrix} \tag{16}$$

In formula (16), $g=\left[-A_0\omega^{-2},0\right]^T$; $A_{11}=\lambda+W1$, $A_{12}=\lambda-W1$;

$$A_{2i,2i-1}=\lambda+Wi\times e+\ i(x_i),A_{2i,2i}=\lambda-Wi\times e-\ i(x_i)$$

$$A_{2i,2i+1}=-\lambda+W(i+1)\times e+\ i+1(x_i),A_{2i,2i+2}=-\lambda-W(i+1)\times e-i+1(x_i)$$

when i=1,2,…n-1,

$$A_{2i+1,2i-1}=(\lambda+\ Fi-\lambda_{Fi})\times e+\ i(x_i),A_{2i+1,2i}=(\lambda-Fi-\lambda_{Fi})\times e-i(x_i)$$

$$A_{2i+1,2i+1}=-\lambda+\ F(i+1)\times e+\ i+1(x_i),A_{2i+1,2i+2}=-\lambda-F(i+1)\times e-i+1(x_i)$$

$$A_{2n,2n-1}=(\lambda+\ Fn-\lambda_{Fn})\times e+\ n(x_n),A_{2n,2n}=(\lambda-Fn-\lambda_{Fn})\times e-n(x_n)$$

3. Calculation of Output Voltage

The straight beam in figure.1 is a composite beam, that attaches PZT piezoelectric coating and Cu electrode on the upper and lower surfaces of Si base beam. Its cross section is shown in Figure 2, in which t_b, t_p and t_e refer to the the thickness of Si beam, PZT material and Cu electrode respectively， b is the width of beam.

When the piezoelectric composite beam suffers a bending deformation, it's assumed that the composite layers are tightly bonded without relative slip, then the longitudinal normal stress in the PZT piezoelectric material will generate the piezoelectric effect, its electric displacement D_3 on the y direction is :

$$D_3 = \varepsilon_{33} E_3 + d_{31} \overline{\sigma_p} \tag{17}$$

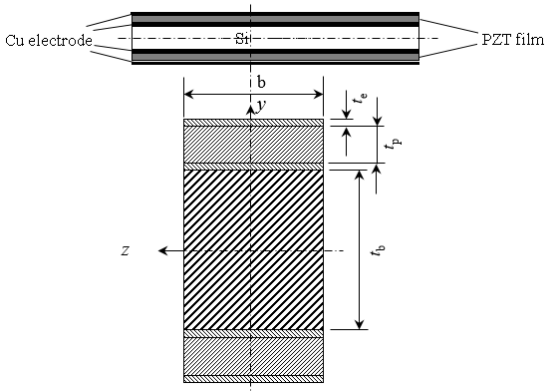

Figure 2 Layered Structure of Symmetrical Cross Section Piezoelectric Composite beam

In the formula (17), ε_{33} and d_{31} respectively refer to the dielectric constant and piezoelectric constant of PZT material, E_3 is the electric field intensity and $\overline{\sigma_p}$ refers to the mean normal stress of PZT piezoelectric material.

When PZT piezoelectric material is used for voltage output, the electric field intensity E_3 =0. Combined with formula (17), it will be:

$$D_3 = d_{31} \overline{\sigma_p} = E_p d_{31} \overline{t_p} w_{i,xx}(x,t) \tag{18}$$

In formula (18), $\overline{t_p}$ refers to the distance between the middle surface of PZT piezoelectric material to the neutrosphere.

Therefore, the Cu electrodes on the upper and lower PZT layer will generate a charge accumulation $Q_i(t)$ as following:

$$Q_i(t) = \int_{x_{i-1}}^{x_i} D_3(x,t) \cdot b \cdot dx = E_p d_{31} b \overline{t_p} \left[w_{i,x}(x_i,t) - w_{i,x}(x_{i-1},t) \right] \tag{19}$$

Taking formula (10) into formula (19), we can get:

$$Q_i(t) = E_p d_{31} b \overline{t_p} e^{j\omega t} \begin{Bmatrix} \left[-j\lambda_i \left(e^{-j\lambda_i x_i} - e^{-j\lambda_i x_{i-1}} \right) \quad -\lambda_i \left(e^{-\lambda_i x_i} - e^{-\lambda_i x_{i-1}} \right) \right] \boldsymbol{C}_i^+ \\ + \left[j\lambda_i \left(e^{j\lambda_i x_i} - e^{j\lambda_i x_{i-1}} \right) \quad \lambda_i \left(e^{-\lambda_i x_i} - e^{-\lambda_i x_{i-1}} \right) \right] \boldsymbol{C}_i^- \end{Bmatrix} \tag{20}$$

Defining C_s as the equivalent capacitance of Cu electrodes on the upper and lower PZT layer, then $C_s=\varepsilon_{33} b(x_i-x_{i-1})/t_p$, the voltage $U_i(t)$ of Cu electrodes can be described as:

$$U_i(t) = \frac{Q_i(t)}{C_s} = \frac{E_p d_{31} t_p \overline{t_p}}{\varepsilon_{33}(x_i - x_{i-1})} e^{j\omega t} \left[\left(\boldsymbol{\Lambda}_i^+ \right)^T \boldsymbol{C}_i^+ + \left(\boldsymbol{\Lambda}_i^- \right)^T \boldsymbol{C}_i^- \right] \quad (i = 1,2) \tag{21}$$

In formula (21), $\boldsymbol{\Lambda}_i^+ = \begin{bmatrix} -j\lambda_i \left(e^{-j\lambda_i x_i} - e^{-j\lambda_i x_{i-1}} \right) \\ -\lambda_i \left(e^{-\lambda_i x_i} - e^{-\lambda_i x_{i-1}} \right) \end{bmatrix}$ $\boldsymbol{\Lambda}_i^- = \begin{bmatrix} j\lambda_i \left(e^{\lambda_i x_i} - e^{\lambda_i x_{i-1}} \right) \\ \lambda_i \left(e^{\lambda_i x_i} - e^{\lambda_i x_{i-1}} \right) \end{bmatrix}$

As for the energy harvester that has a segmentation structure in figure.1 and a cross section shape of figure 2, its total output voltage can be described as:

$$U(t) = 2\sum_{i=1}^{n} U_i(t) = \frac{2E_p d_{31}}{\varepsilon_{33}} e^{j\omega t} \sum_{i=1}^{n} \left\{ \frac{t_{pi}}{x_i - x_{i-1}} \left(\frac{t_{bi} + t_{pi}}{2} + t_e \right) \left[\left(\boldsymbol{\Lambda}_i^+ \right)^T \boldsymbol{C}_i^+ + \left(\boldsymbol{\Lambda}_i^- \right)^T \boldsymbol{C}_i^- \right] \right\} \tag{22}$$

4. Performance Analysis

In order to verify the feasibility of the optimization scheme mentioned above, a new harvester whose n equals to 2 has been taken in this part for numerical analysis, as shown in figure.3. The influence of

upper and lower Cu electrodes will be ignored, namely $t_{e11}=t_{e12}=t_{e21}=t_{e22}=0$. PZT-5H is selected as the piezoelectric material that is only pasted on one side of SI beam, namely $t_{p2}=0$. With b_1、t_{b1}、t_{p11}、b_2、t_{b2}、t_{p12}respectively refer to the width and thickness of beam 1 and 2.

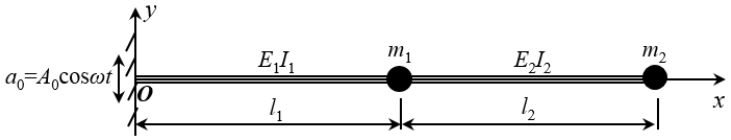

Figure 3 Diagram of Two Beams' Harvester

Table 1. Geometric Parameters of Harvester When n=2

Name	l_1 mm	l_2 mm	m_1 kg	m_2 kg	b_1 mm	b_2 mm	t_{b1} μm	t_{b2} μm	t_{p11} μm	t_{p12} μm
Value	15	6	$1*10^{-6}$	$1.7*10^{-6}$	1	1.8	8	13	3.3	6.2

According to parameters in table 1, the charge quantity and voltage of each beam generated from its deformation are taken as the research object to analyze the changes along the frequency.

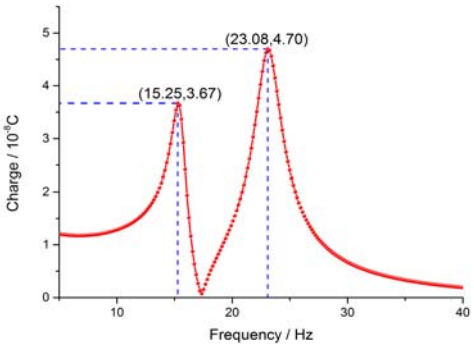

a) Charge-Frequency Curve of PZT-5H

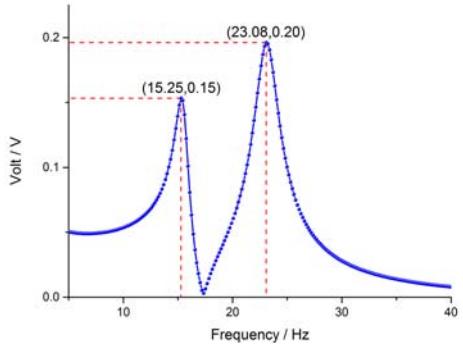

b) Voltage-Frequency

Figure 4 Variation Curve of Charge Along With the Voltage on Beam 1

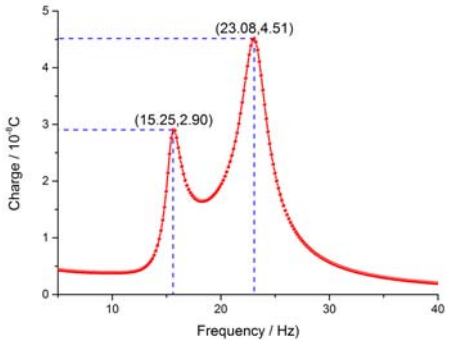

a) Charge-Frequency Curve of PZT-5H

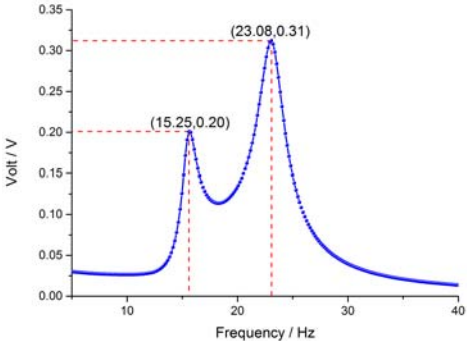

b) Voltage-Frequency

Figure 5 Variation Curve of Charge Along With the Voltage on Beam 2

Comparing figure 4 and 5, we know that the peak value of charge quantity and voltage for the two beams appear at the frequency 15.25Hz and 23.08Hz, namely the two frequencies are the resonant frequency of harvester. When the frequency is 15.25Hz, the charge quantity of beam 1 is $3.67*10^{-8}$C, and its output voltage is 0.15V. The charge quantity of beam 2 is $2.90*10^{-8}$C, corresponding output

voltage is 0.20V. When the frequency is 23.08Hz, the charge quantity of beam 1 is $4.70*10^{-8}$C, and its output voltage is 0.2V. The charge quantity of beam 2 is $4.51*10^{-8}$C, corresponding output voltage is 0.31V.

The new harvester takes each beam as a micro harvester, and two micro harvesters are connected in series, so the charge quantity and output voltage of the whole beam equal to the sum of that on the two beams respectively. The simulation results also proved this relationship, When the frequency is 15.25Hz, the output voltage of harvester is 0.35V, when the frequency is 23.08Hz, the output voltage is 0.51V. If the effective value of output voltage is 80mV, then the energy harvester has two frequencies with in a frequency scope of 10Hz~50Hz, which are 9.63Hz and 29.95Hz. The harvester also forms an effective operating frequency band between the two frequencies, which is 20.32Hz.Thus it can be seen that the new energy harvester consisted of two beams and two mass blocks indeed meets the demand of reducing resonant frequency and broadening working band. It can match the low frequency vibration environment more perfectly and provide sufficient power for the equipment to be supplied.

5. Conclusion

This paper designed a new structure consisted of n beams and n mass blocks, that can meet the demands of reducing resonant frequency and broadening working band. Considering the scale effects, transverse vibration displacement of each beams have been solved, the calculation formula of output voltage and flexural rigidity of cross section for the new harvester have been derived with external excitation. Meanwhile, an example has been taken when n=2, the change laws of concentrated charge and output voltage for PZT-5H surface along the frequency have been analyzed.There are two resonant frequencies within 50Hz(namely 15.25Hz and 23.08Hz) that can better match the low frequency ambient vibration. When the output voltage is 80mV, the effective working band of harvester is 20.32Hz. The resonant frequency and working band of this harvester are optimized. Moreover it can adjust the parameters according to actual power demand, which greatly optimizes the performance of micro power supply and better meets the energy supply requirements of the equipment to be supplied.

References

[1] Kuehne I, Frey A Marinkovic D 2008 *Sensors and Actuators* A: *Phys* **142(1)** 263-269
[2] Roundy S, Wright P K, Rabaey J 2003 *Computer Communications Ubiquitous Computing* **26(11)**1131-1144
[3] Piezoelectric energy converter for electronic implants 1969 *Google Patents*
[4] Jeon Y B, Sood R, Jeong J H, et al. 2005 *Sensors and Actuators* A *Phys* **122(1)** 16-22
[5] WU Xiao-ming, FANG Huan-jun, LIN Jian-hui, et al. 2008 *Journal of function materials and devices* 14(2)
[6] Renaud M, Karakaya K, Sterken T, et al. 2008 *Sensors and Actuators* A: *Phys* 145–146, 380-386
[7] Gafforelli G, Ardito R, Corigliano A 2015 *Composite Structures* **127(0)** 369-381
[8] Fang H, Liu J, Xu Z, et al 2006 *Microelectronics Journal* **37(11)**: 1280-1284
[9] Trawiński W, Bobiński J, Tejchman J 2016 Engineering *Fracture Mechanics* 168 Part A, 204-226
[10] LIU Ying, WANG YAN-fen, LI Guang 2014 *Optics and Precision Engineering* **22(9)**:2476-2482
[11] Zhidong W, Rui H, Daokun Z 2016 *Piezoelectric and Acoustooptics* 320-323